Available online at www.sciencedirect.com
ScienceDirect
C. R. Physique 7 (2006) 858–874
COMPTES RENDUS
PHYSIQUE
http://france.elsevier.com/direct/COMREN/

Ultimate lithography/Lithographie ultime

Optical lithography—present and future challenges

Burn J. Lin

TSMC, Ltd., Hsinchu, 300-77 Taiwan, ROC

Abstract

Optical lithography has been an industrial workhorse for many decades. It has reached a wavelength of 193 nm, a Numerical Aperture (NA) of 0.93 but was facing difficulties to advance further until the debut of immersion lithography. This review deals with the limit of dry and immersion lithography systems, their present and future challenges to reach these very limits. A discussion of defects in immersion lithography, the status of immersion lithography, polarized illumination, high-index materials, solid-immersion mask, double exposure and double patterning is included.***To cite this article: B.J. Lin, C. R. Physique 7 (2006).***
© 2006 Académie des sciences. Published by Elsevier Masson SAS. All rights reserved.
Résumé

Lithographie optique—défis présents et futurs. La lithographie optique a été la technologie industrielle par excellence depuis plusieurs décennies. Elle est arrivée jusqu'à une longueur d'onde de 193 nm et une ouverture numérique de 0,93 et elle rencontrait des difficultés pour progresser plus avant jusqu'à l'entrée en lice de la lithographie en immersion. Cet article traite des limites des systèmes de lithographie sèche et en immersion, des défis présents et futurs pour pousser à l'extrême limite cette technique. Est incluse une discussion sur les défauts en lithographie par immersion, le point sur cette lithographie en immersion, l'illumination polarisée, les matériaux à fort indice de réfraction, les masques à immersion solide, la double exposition et la double impression. ***Pour citer cet article : B.J. Lin, C. R. Physique 7 (2006).***
© 2006 Académie des sciences. Published by Elsevier Masson SAS. All rights reserved.

Keywords: Microlithography; Optical lithography; Immersion lithography

Mots-clés : Microlithographie ; Lithographie optique ; Lithographie en immersion

1. Introduction

Optical lithography started with IC fabrication. The earliest form used cut-and-paste with scissors to make an emulsion mask and a visible light source to replicate its image. In a few decades, the resolution has been reduced from tens of micrometers to hundredths of a micrometer. Mask-making tools evolved from scissors to optical pattern generators, e-beams, laser beams, and spatial light modulators. The replication tools evolved from contact printing to projection printing, reduction systems, step-and-repeat systems, and step-and-scan systems. The reduction of wavelength, increase in NA, and development of resolution enhancement techniques reflected in the reduction of the resolution

E-mail address: burnlin@tsmc.com (B.J. Lin).

1631-0705/$ – see front matter © 2006 Académie des sciences. Published by Elsevier Masson SAS. All rights reserved.
doi:10.1016/j.crhy.2006.10.005

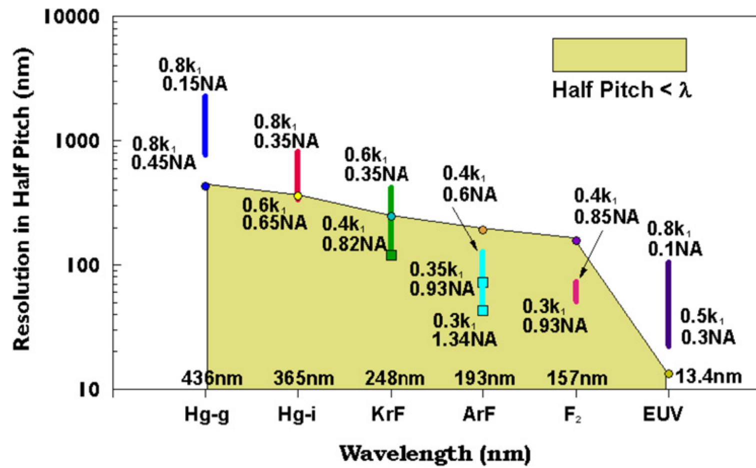

Fig. 1. Evolution of projection optical lithography from 436 nm, 0.15 NA, 0.8 k_1 to 193-nm immersion.

scaling factor k_1 are depicted in Fig. 1. It started from the 0.15-NA 436-nm g-line lens featuring a resolution of over 2 μm, using a $k_1 \equiv (\text{half pitch} * \text{NA})/\lambda = 0.8$, by raising NA until the lens became too expensive to build at that time, by reducing the wavelength to reposition the NA for the next round of increase, and lowering k_1 whenever the pace of NA and wavelength changes fell behind the circuit shrinking roadmap. This trend continued through wavelengths of 365, 248, and 193 nm and was continuing into 157 and 13.5 nm. Note that the half-pitch resolution quickly became subwavelength as early as 365-nm wavelength at 0.55 NA and 0.5 k_1. Opportunity for larger-than-wavelength imaging will reappear only at the 13.5-nm wavelength.

Currently, the IC industry is on the verge of manufacturing the 45-nm node at 65-nm half pitch, using water-immersion ArF lithography at 1.2 NA. With 1.35 NA, there is the possibility of manufacturing the 32-nm node at 45-nm half pitch. From this point in time, we are less likely to further improve resolution while maintaining a usable depth of focus (DOF), unless much more radical techniques are used. One less radical technique is to continue immersion lithography, using a fluid with refractive index higher than that of water. The challenge is shifted from the optical system to materials, even though one still requires a higher aperture angle at the reticle side. Staying with water immersion, there is no room for improvement in the optical system, because the sine of the aperture angle at the wafer side is already in the 0.95 regime. The only way to resolved 32-nm half pitch is to split the pitch into larger ones and recombine for the required pitch by double processing. The challenge is on the economical side, as well as in overlay accuracy. Split pitch can be applied to dry scanners such as 193-nm 0.93-NA. At $k_1 = 0.15$, the resolution is sufficient to handle 32-nm half pitch. So, why does one not use dry lithography, such as 13.5-nm Extreme Ultra Violet (EUV) lithography? Of course, EUV lithography operating at $k_1 > 0.5$ brings us back to the same comfort as manufacturing the 180-nm half pitch using 193-nm light at 0.65 NA. However, EUV lithography has its own problems to overcome. This brings us to a dark horse, namely, multiple e-beam direct-write. Despite its throughput handicap, with the escalating mask cost and the absence of pellicle for EUV lithography, it may turn out to be the most economical and feasible for 32-nm half pitch and below.

This report deals with the present and future challenges of optical lithography. We will limit the discussion to 193-nm lithography. We first show the limit of dry lithography, then the reasons to go to immersion lithography. We then discuss the most urgent challenge to turn 193-nm immersion lithography into a manufacture-worthy process, aiming at 65-nm half pitch, 45-nm logic node. From this point the challenge is in using it for smaller half pitches. We will report the progress in 193-nm immersion lithography, the problems it is encountering, and potential solutions, followed with methods to extend 193-nm immersion lithography to its ultimate potential.

2. Basic considerations

2.1. Limit of 193-nm dry lithography

The performance of an optical imaging system is characterized by three major parameters, resolution, depth of focus (DOF), and overlay accuracy.

Resolution is generally determined by the $\mathrm{NA}/\boldsymbol{\lambda}$ ratio, multiplied by k_1, where NA is the numerical aperture of the imaging lens; $\boldsymbol{\lambda}$, wavelength; k_1 the resolution scaling factor which indicates the relative resolution based on a given $\mathrm{NA}/\boldsymbol{\lambda}$ ratio. Generally, $k_1 = 0.8$ or higher is considered an easy point of operation for optical lithography. Some of the manufacturing reference points using such k_1 are seen in Fig. 1. This operating point was adopted when optical lithography was used without much intelligence. Pattern corners suffered from little aesthetically-objectionable rounding, line ends did not shorten, optical proximity correction (OPC) was not needed. Soon after, it was realized that high-k_1 is uneconomical, using high $\mathrm{NA}/\boldsymbol{\lambda}$ ratios unnecessary [1,2]. After recovering lost resolution by managing multiple reflections and vibrations, the k_1 factor was reduced to 0.5–0.6. At this level, corner rounding and line end shortening are minimal. OPC is rarely needed unless line/space and hole/island patterns are mixed. To further squeeze tool performance, k_1 has been dropped to 0.4 for logic circuit manufacturing and as low as 0.35 for memory circuits with resolution enhancement techniques (RET) such as phase shifting mask (PSM) and off-axis illumination in conjunction with heavy OPC. Memory circuits are produced in much large quantities per mask. They can afford extreme customisation in RET. Fig. 1 also shows the progression of CD from larger-than-wavelength to smaller-than-wavelength. $W/\lambda = k_1/\mathrm{NA}$ indicates W normalized to λ. It is not a true indicator of the difficulty of practicing optical lithography. For example, $W = 0.55\lambda$ can be achieved with $k_1 = 0.5\lambda$ at $\mathrm{NA} = 0.93$, which is not really very difficult. On the other hand, $W = 0.55\lambda$ can be very difficult if $\mathrm{NA} = 0.5$ instead of 0.93, because k_1 becomes 0.275.

The DOF of an optical imaging system is determined by two considerations. The first consideration is on diffraction DOF, the DOF supported by imaging, i.e. the DOF of the diffracted image from the common exposure-defocus (E-D) window of a given set of critical features using a given RET condition based on the $\mathrm{NA}/\boldsymbol{\lambda}$ ratio of the imaging lens. The effect is summarized by the non-paraxial DOF scaling coefficient k_3 to be multiplied with $\boldsymbol{\lambda}/\sin^2(0.5\boldsymbol{\theta})$ where $\boldsymbol{\theta}$ is the aperture angle of the imaging lens. The other consideration for DOF is the available DOF, which is $\mathrm{DOF_{diff}}$ with contribution from the resist thickness removed. $\mathrm{DOF_{avail}}$ is the allowance for tool, wafer, and mask contributions to DOF. These contributions include image plane deviation and astigmatism from the lens, vertical imperfections in scanning, wafer and mask tilt, lack of flatness from wafer and mask, wafer and mask topography, errors in metrology in the vertical direction, etc. As resolution is reduced, $\mathrm{DOF_{diff}}$ becomes smaller. $\mathrm{DOF_{avail}}$ follows.

The relationship of resolution and $\mathrm{DOF_{diff}}$ to half pitch, NA, and $\boldsymbol{\theta}$ can be summarized by the scaling equations of resolution and $\mathrm{DOF_{diff}}$, according to Ref. [3].

$$\mathrm{MHP} = k_1 \frac{\lambda}{\sin\theta} \tag{1}$$

$$\mathrm{DOF_{diff}} = k_3 \frac{\lambda}{\sin^2\frac{\theta}{2}} \tag{2}$$

where MHP is the minimum half pitch. Note that λ and θ have to be taken in the same medium. The situation of DOF in two media is complicated. Readers are referred to Ref. [4].

The overlay accuracy is usually required to be 1/3 of the minimum CD. Contributions to overlay inaccuracy include alignment errors, magnification error, rotational error, skew, mask feature placement error, and stage accuracy. It takes on new significance due to immersion lithography, double exposure and double patterning.

For 193-nm dry system, the theoretical limit of NA is 1. Practically, 0.93 is already quite difficult and expensive. The leverage of further increasing it is low. Design and construction of the imaging lens will be extremely difficult and the size will be large. Because the improvement in resolution in inversely proportionally to NA, the improvement from 0.93 to 0.99 is only 6%. Staying at 0.93 NA and $k_1 = 0.3$, the resolution in 63-nm half pitch can be supported. Double processing at $k_1 = 0.15$ brings the half pitch down to 32 nm. However, it is more reasonable to switch to immersion lithography at a higher k_1 before dropping it to 0.3 and 0.15. This way, the DOF and the mask error factor (MEF) are more favourable for manufacturing. They will be brought down only at the last resort, especially for logic products, which have more design variations and cannot be tailored as closely as memory products.

2.2. Reasons for immersion lithography

Immersion lithography works by filling the space between the last lens surface and the photoresist with a fluid, as shown in Fig. 2. With the fluid, high spatial frequencies from the lens can be coupled to the photoresist. The performance of an immersion system can be evaluated with Eqs. (1) and (2) by letting $\boldsymbol{\lambda} = \boldsymbol{\lambda}_0/n$, where n is the refractive index of the coupling medium. Of course, the aperture angle $\boldsymbol{\theta}$ has to be taken in the same medium as the wavelength

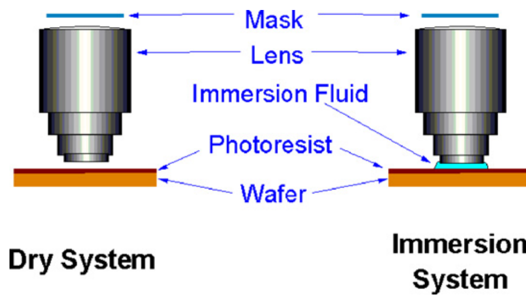

Fig. 2. Schematic immersion imaging system. The space between the last lens surface and the photoresist on wafer is filled with a fluid to increase the refractive index of this space.

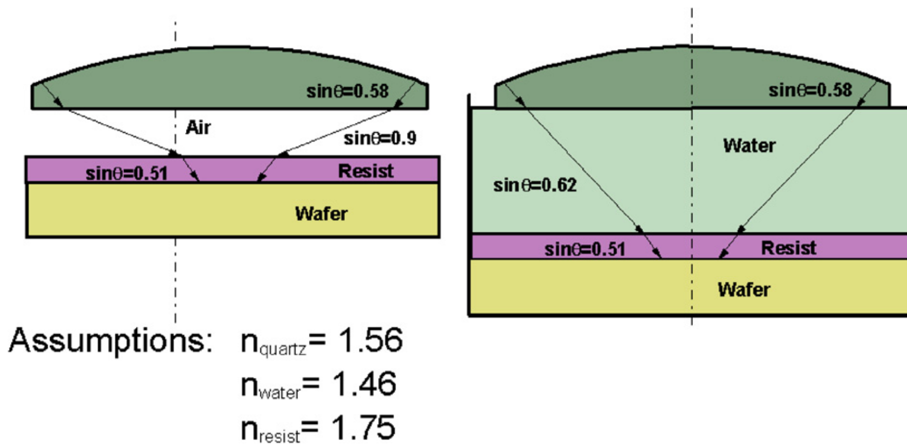

Fig. 3. Preserving the incident angle in resist to improve DOF.

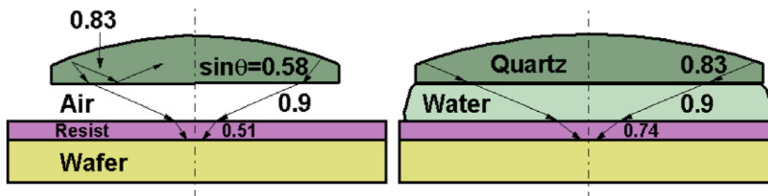

Fig. 4. Preserving the physical angle in coupling medium to improve resolution.

is taken from. It is similar to reducing the wavelength of the imaging system. As the wavelength is reduced, the resolution is improved proportionally, when $\boldsymbol{\theta}$ is made identical to $\boldsymbol{\theta}_0$. In this case, the DOF is also reduced proportionally. At constant resolution, the immersion DOF is improved more than proportional to the refractive index change, because $\sin^2\theta/2$ changes more than the change of refractive index. Generally speaking, by adjusting θ, resolution and DOF can be traded off against each other with a net gain with respect to the resolution-DOF combination from a dry system. The refractive index of water is 1.44. Using it as the immersion fluid at aperture angle $\sin\theta = 0.93$ makes the NA 1.34. With a high-index fluid of $n = 1.65$, $\mathrm{NA} = 1.53$ can be achieved.

An example is shown in Fig. 3 using $\sin\theta_{\mathrm{resist}} = 0.51$, and refractive indexes 1.56, 1.44, and 1.75 for the lens material, water, and resist, respectively. Simple Snell's law calculations set $\sin\theta_{\mathrm{quartz}} = 0.58$, $\sin\theta_{\mathrm{air}} = 0.9$, and $\sin\theta_{\mathrm{water}} = 0.62$. If the image were to be recorded in the coupling medium, Eq. (2) predicts a gain in $\mathrm{DOF}_{\mathrm{diff}}$ of 96%. It is much larger than the DOF obtained by just multiplying with the refractive index, as just explained. An immersion system that preserves the physical angle in the coupling medium is shown in Fig. 4, using the same distribution of refractive indexes as in Fig. 3. The resolution is now improved by 46%, while DOF is reduced by 46%, according to Eqs. (1) and (2).

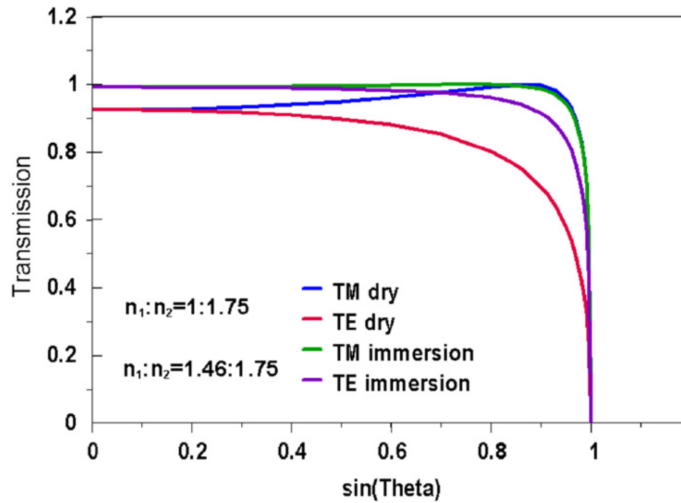

Fig. 5. Transmission in TE and TM modes, dry (index of refraction of air $n_1 = 1$) and immersion (index of refraction of water $n_1 = 1.46$) systems with a photoresist index of refraction $n_2 = 1.75$.

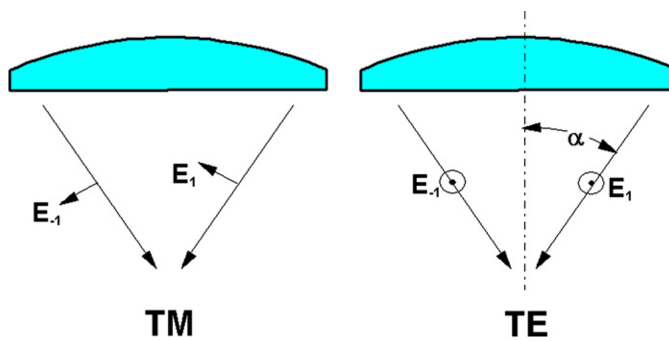

Fig. 6. TM and TE light.

Another advantage of immersion lithography is the reduction of stray light and unwanted polarization due to better index matching between the lens and the resist. The transmission of obliquely incident light into the resist, with incident angle θ with respect to the normal to the resist surface is plotted in Fig. 5. From air to the resist, as in a dry system, the transmission is lower than that from water to the resist, especially for transverse-electric (TE) field. The transverse-magnetic (TM) and TE fields are depicted in Fig. 6. Because the electric field vectors of the latter remain always in the same direction regardless of change incident angle, they can recombine without loss of contrast and are preferred over the former. Unfortunately, a dry system tends to transmit more of the unwanted polarization into the resist.

One is reminded that wavelength reduction in the medium by refractive index change is exhibited in the change of velocity of light in the medium. The frequency of the light wave is not changed. As given by the well known equation on photon energy,

$$E = h\nu \tag{3}$$

where E is the energy of a photon; h, Planck's constant; and ν, the frequency of the light wave. The energy of the light wave, and thus the characteristics of interaction with the materials, are unchanged in any light-transmitting medium. The mask, the lens, and the resist materials are illuminated with the same light frequency. Even the light source emits the same frequency. Hence, they do not have to be treated differently; whereas, a change of the vacuum wavelength changes the frequency. It requires new materials to work in the new frequency.

3. Present challenges in immersion lithography

Immersion lithography is much more difficult than immersion microscopy, even though they use the same optical principle. For the latter, the image field is much smaller, image distortion resulting in overlay errors, defects, and throughput is never of prime importance. With immersion lithography, the fluid has to be extremely homogeneous even under intense illumination of the patterning light, while the wafer is moving at a high speed with respect to the imaging lens. The temperature of the fluid also has to be controlled very stringently to maintain a constant refractive index. Fluids tend to leave stains, generate bubbles, and carry particles around, thus, generate defects on the wafer. Temperature variations in the immersion fluid, either due to inhomogeneities or inconsistencies can lead to overlay errors, focussing errors, and aberrations. Handling defects and temperature variations often lead to trade offs with wafer throughput. We now concentrate on immersion-related defects and their reduction, which leads also to better overlay and throughput. Other aspects such as overlay and throughput improvement are the expertise and responsibilities of exposure-tool manufacturers.

The immersion-related defects can be classified as printed bubbles, water stains, printed particles, and fall-on particles as shown in Fig. 7. Bubbles are mostly generated from turbulence. They are usually micrometers in size, because smaller bubbles readily dissolve in the immersion fluid, which has been heavily degassed. Water stains result from wet residue escaping the confinement of the immersion hood as the wafer scans pass the lens assembly. When a particle is on the resist surface during exposure, its image is permanently recorded in the resist. It is a printed particle. If the particle falls on the wafer after the location is exposed, it is simply a fall-on particle.

A schematic immersion assembly is shown in Fig. 8. The lens and the immersion hood are near the wafer edge. At the inevitable gap between the wafer edge and the wafer chuck, turbulence tends to produce bubbles. Particles can be washed into the gap and accumulated there if the flow rate is too slow. They can be washed back to the wafer surface. With a faster flow rate, this type of defects can be reduced but at the expense of worsening overlay, because of uneven wafer cooling. Attempts of local heating to compensate for the heat loss are extremely difficult. In addition to turbulence, backwashing, and cooling, the edge of the resist after edge bead removal, shown in Fig. 9, tends to be broken off by the water flow, becoming another source of particles.

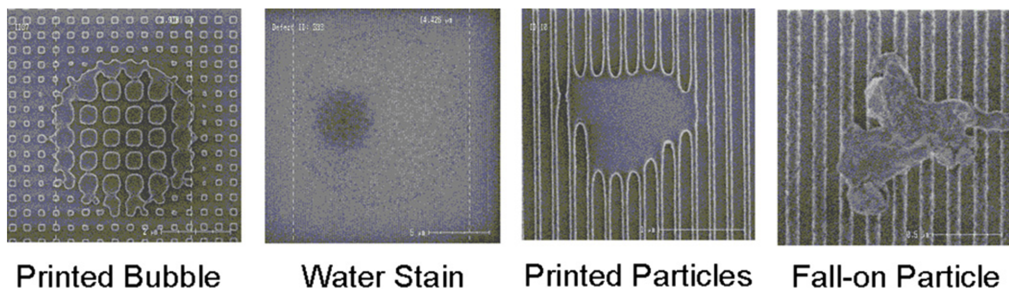

Fig. 7. Types of immersion-related defects.

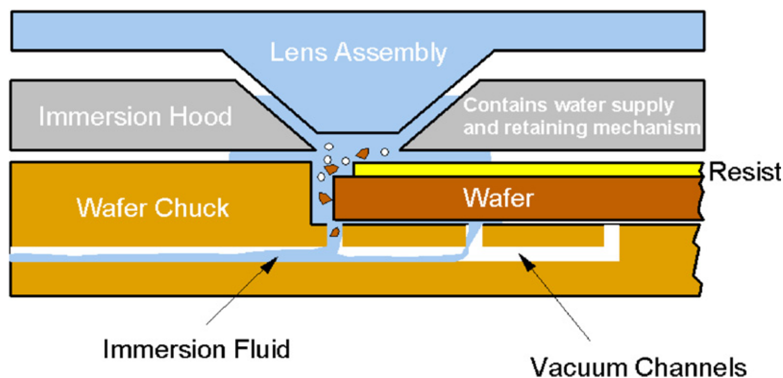

Fig. 8. Fluid flow in an immersion assembly.

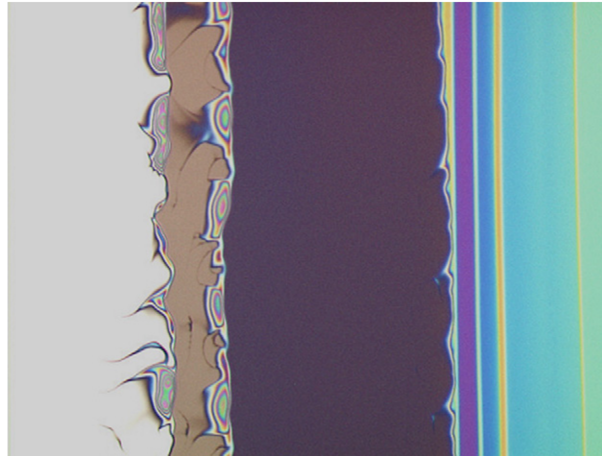

Fig. 9. Resist edge after edge-bead removal.

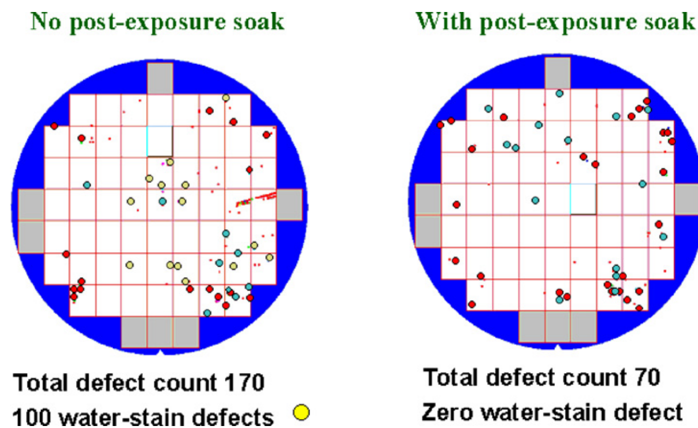

Fig. 10. Number of water stain defects reduced by post-exposure soak.

A straightforward way to reduce water stain is to perform a post-exposure soak before baking so that any precipitation is re-dissolved and washed away. A typical post-exposure soak result is shown in Fig. 10. The number of defects was reduced from 170 to 70. However, when the water stain is left on the wafer for too long, a post-exposure soak cannot completely remove water-stain related defects. Some scanners rely on high hydrophobicity to prevent water-stains [5]. It limits the choice of resists. Of course, there are other ways to optimise the resist characteristics to prevent water-stains. A trivial way to guarantee freedom from water-stains is to adopt the wafer-based immersion scheme [6] where the entire wafer is immersed through the entire exposure process.

Stationary and moving defects are quantified with a multiple-exposure technique as shown in Fig. 11. By splitting a normal 39-$\mathrm{mJ/cm^2}$ exposure into 2, 3, 4, and 5 exposures, one identifies that only 20 of the 85 defects are stationary. The signature of defects is evaluated with superposition of many defect maps. The defect distribution shown in Fig. 12 is the superposition of the defect map of 20 bare-Si wafers. There are distinct partial circles and straight-line sections attributed to particles released from parts of the immersion hood. These particles are outside of the exposure field but can be printed later, if they remain undisturbed when the wafer moves them under the exposure field in the subsequent step-and-scan sequence. Special step-and-scan sequences, call routing [7], as shown in Fig. 13, can reduce the number of printed particles. Here the particles capable of being printed are called effective residues; the others, ineffective residues. Normal routing, though more efficient, produces many printed particles. Those effective residues in field 5 will be printed when the wafer moves field 5 under the lens and the immersion hood (IH). With special routing 1, half of the effective residues are eliminated. With special routing 2, all effective residues, except those few left in field 6 and subsequently those in fields 5 and 4, are rendered ineffective. Wafers processed this way as a final step of all

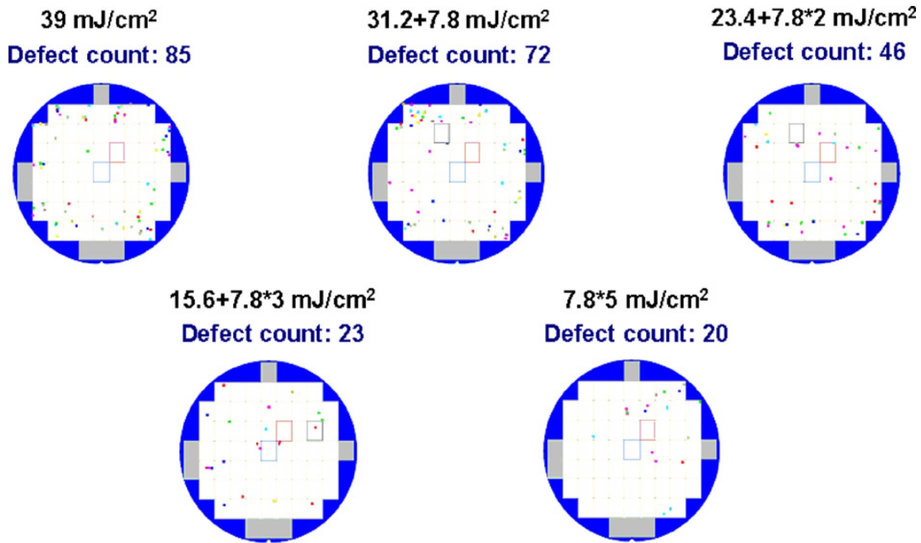

Fig. 11. Immersion defect study using 1 to 5 exposures, each totalling 39 mJ/cm^2.

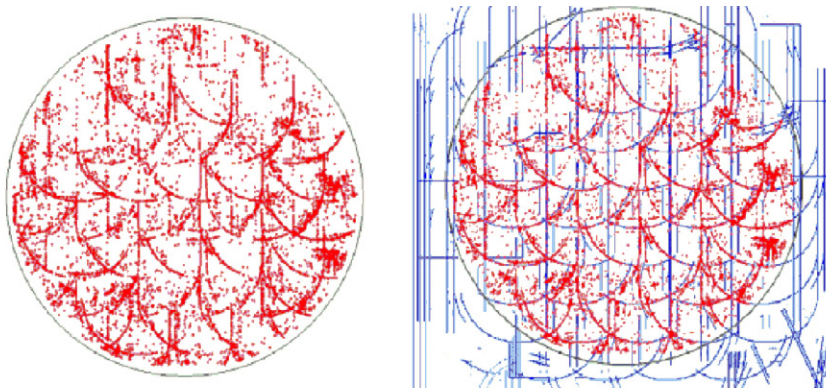

Fig. 12. Immersion defect study by accumulating the defect map of 20 bare-Si test wafers.

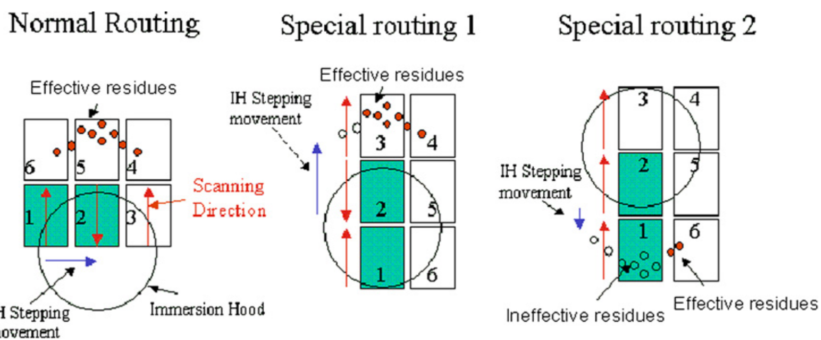

Fig. 13. Normal and special routings for immersion lithography. The immersion hood (IH) is shown as a circle.

defect reduction measures, have single digit defect numbers. In a typical batch, the average number of defects is 4.8 per wafer. Among them, there are three wafers with just 1 defect; two, with 2 and 3. Obviously, special-routing-2 trades off wafer throughput. The throughput loss is about 15%.

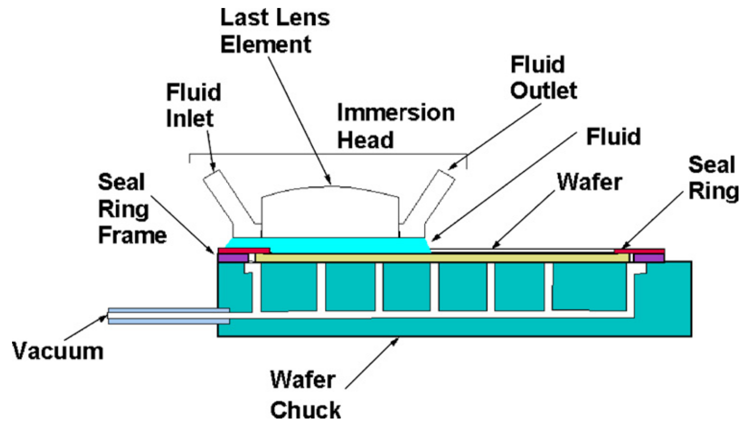

Fig. 14. Wafer chuck supporting edge seal ring on seal ring frame. Frame and wafer are substantially coplanar.

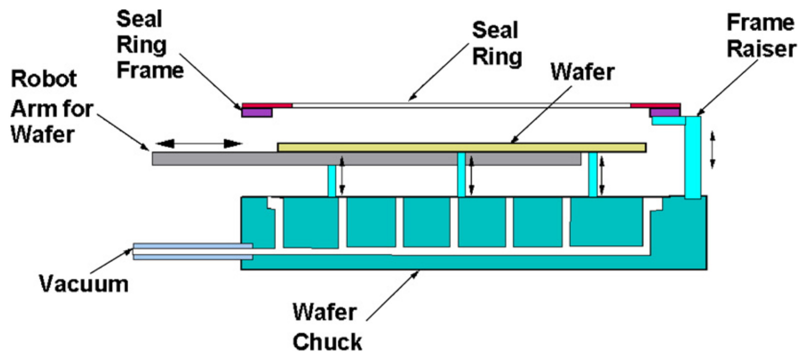

Fig. 15. Seal ring and seal ring frame raised above wafer, which is lifted by pins to allow robot arm to load and unload wafer to the wafer chuck.

By far the most effective method to reduce defects would be to place a wafer seal ring at the edge of the wafer as shown in Fig. 14. The seal ring is a thin flexible material like that of a mask pellicle. It is supported by the seal-ring frame, which is practically co-planar with the wafer surface. The seal ring is secured by vacuum to seal off the wafer edge from fluid flowing through it. It eliminates turbulence when the IH is at the wafer edge. Particles will not fall into the space between the wafer and the wafer chuck, accumulating there to be subsequently back-washed. There is no longer uneven cooling from the immersion fluid flowing through the wafer edge, leading to overlay inconsistency. The seal ring also suppresses the resist border at the wafer edge to prevent any peel off of resist as a particle source. The seal ring and the supporting frame can be raised above the wafer during wafer loading and unloading as shown in Fig. 15. They can be easily replaced or cleaned. This measure, in conjunction with cleanliness control of the IH and its periodic cleaning, will ensure very low defect density for immersion lithography. A typical overlay vector map is shown in Fig. 16. The chips near the wafer edge have indeed larger overlay errors. With water temperature in check, 'send ahead wafers', by far a dominant throughput killer, can be eliminated. With defect sources gone, special routings will not be needed.

4. Immersion lithography results

193-nm water-immersion has been applied to logic devices and circuits to explore its potential and discover its problems. The polysilicon images shown in Fig. 17 consist of 90-nm-node SRAM overlaid on the active layer [8]. The former was exposed on a 0.75-NA 193-nm immersion scanner and the latter, on an equivalent dry system. It demonstrates full-field imaging, a usable resist system, acceptable overlay, and large DOF. Turning to a 0.85-NA 193-nm immersion scanner, 55-nm node SRAM chips were delineated, and Fig. 18 shows the metal layer image of this chip at different field locations. The number of good-to-bad dies is compared in Fig. 19 in a dry-immersion split at the contact layer. The ratio is 72:70 versus 62:80 despite immersion-induced defects. The improvement of

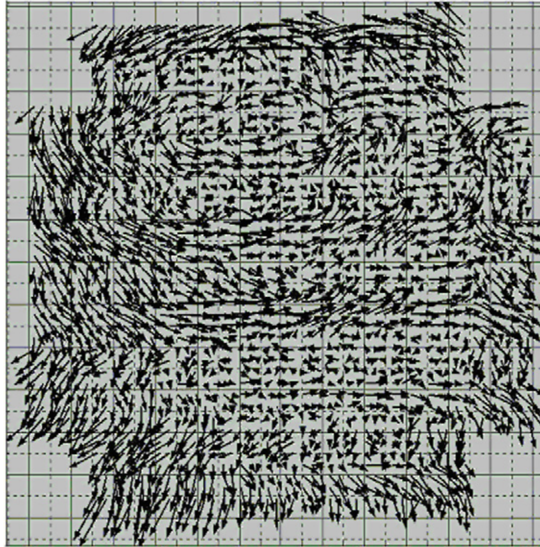

Fig. 16. Typical overlay vector map.

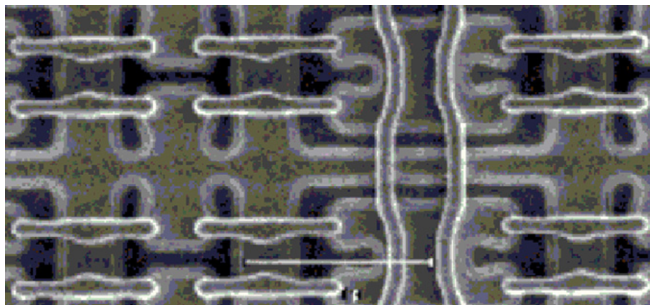

Fig. 17. Immersion chip using 90-nm-node SRAM. The poly-layer overlays on the active layer. The former was exposed with a 0.75 NA 193-nm immersion scanner.

DOF simply outweighs defects. The number of good immersion dies would have been 25 more, attaining 97:45, if a non-photo mis-operation had been properly accounted for.

5. Future challenges

Ref. [6] shows the NA/σ and resolution enhancement techniques that can be employed to reach 45-nm half pitch or the 32-nm logic node. A few more techniques can be used on 193-nm immersion lithography to extend this further, namely by using polarized illumination, higher-index materials, solid mask immersion, and double exposure/patterning.

5.1. Polarized illumination

A light wave propagating with an arbitrary orientation of the electric field vector towards the wafer can be split into TE and TM components as given in Section 2.2. In terms of combination of spatial frequencies, the TE mode is most efficient. All TE spatial frequencies have their electric field vectors collinear to each other. They superimpose completely, leaving no un-combined stray light. With the TM mode, the combination efficiency of the electric field vectors is a function of the incident angle, less efficient with larger angles. The components that do not combine travel in opposite directions and become stray light to reduce the image contrast. When the illumination is restricted to only the TE mode, the image contrast is preserved even at large incident angles.

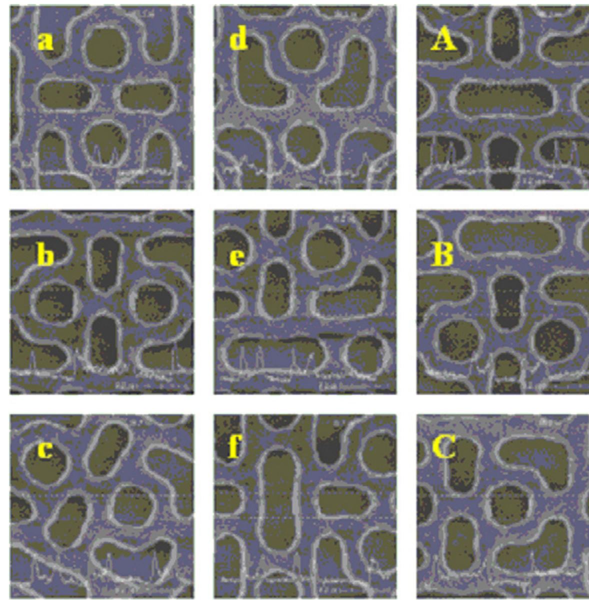

Fig. 18. 0.4-μm^2 cell, 55-nm-node SRAM metal layer exposed with a 0.85 NA 193-nm immersion scanner.

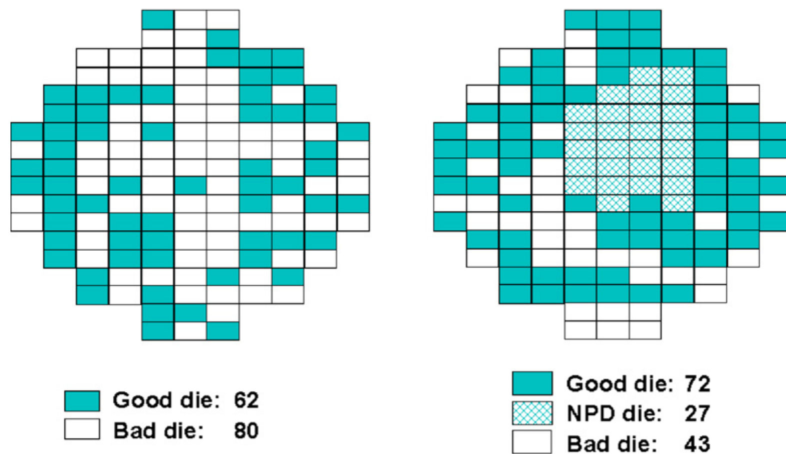

Fig. 19. 65-nm SRAM immersion yield from R&D lot. On the left side the yield map is obtained using dry lithography and on the right using immersion lithography. In the latter case some dies (NPD dies) were defective due to non-lithographic problems.

A schematic drawing of a projection-printing system is shown in Fig. 20, with the spatial frequencies of the imaging light, reflected light, the formation of system stray light (SSL) and polarization dependent stray light (PDS). The illuminating light is split into 0, ±1, ±2 orders by the grating mask. They are scattered by surface roughness and multi-reflected by an imperfect antireflection coating at the lens surfaces. They are also reflected by the mask absorber. All turn into SSL which is polarization-dependent but the effect is not strong because of the averaging effect of many different reflecting surfaces, incident and reflecting angles. The ±2 order beams blocked by the lens aperture may also turn into stray light because of incomplete blocking. Now the 0 and ±1 order beams that transmit and reflect at the resist/wafer and resist/coupling-medium interfaces are strongly polarization-dependent. The TM transmitted beams into the resist do not recombine completely. The reflected TE and TM beams are scattered and multi-reflected by the lens surfaces as well as reflected by the mask absorber just as the incident beams. They induce another level of stray light. The resultant contrast loss leads to reduction in exposure latitude and DOF.

Given 8% exposure latitude, the DOF of 65-nm equal lines and spaces is plotted in Fig. 21 for 193-nm water immersion, 193-nm dry, and 132-nm dry systems [1]. The wavelength 132 nm is used because of the earlier reported

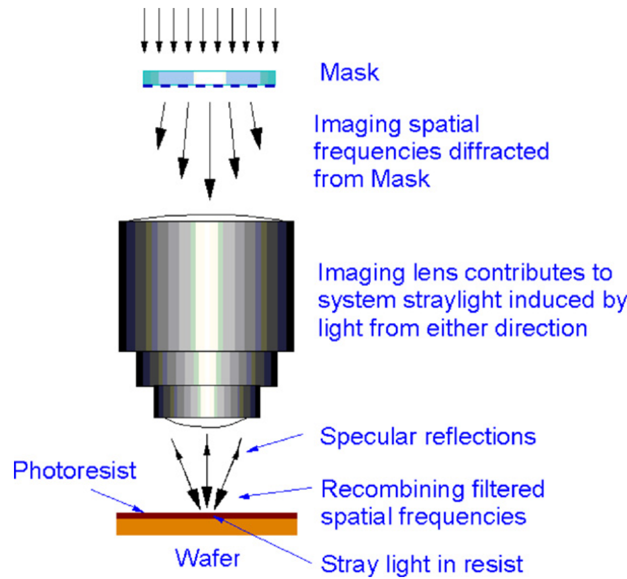

Fig. 20. Imaging light, reflecting light, and stray light.

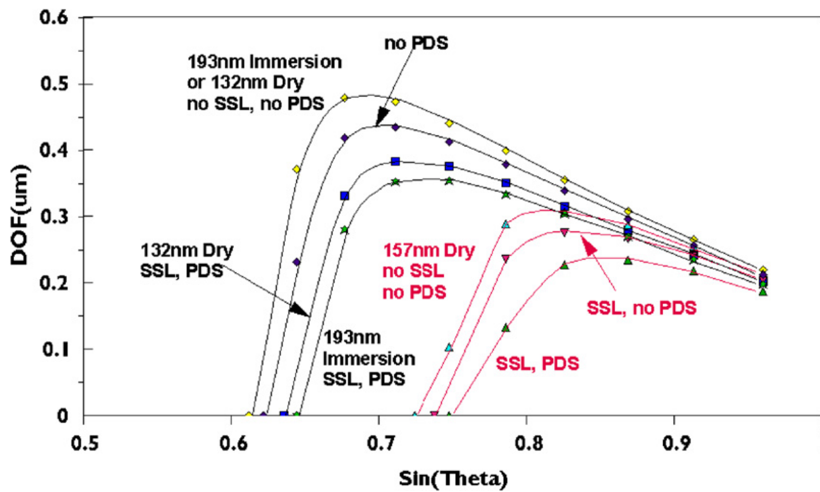

Fig. 21. Effects of stray light. Polarization Dependent Straylight (PDS) from 157-nm and 132-nm dry as well as 193-nm immersion considered for imaging 65-nm lines and openings, at $\sigma = 0.82$, 8% exposure latitude, $n_{\text{immersion fluid}} = 1.46$, $n_{\text{resist}} = 1.75$, CD tolerance $= \pm 10\%$, System StrayLight (SSL) $= 10\%$.

value of refractive index of water [9,10] of 1.46. Since adjusting the wavelength by 1.4% would not produce any perceivable difference in the figure, 132 nm is not updated. The curve with the largest DOF is based on either a perfect 193-nm immersion system or a theoretical 132-nm dry system. As soon as SSL is considered, the DOF drops to the 'no PDS' curve. The DOF drops further with PDS included. The loss is more significant for the 193-nm immersion system than the 132-nm dry system. The worse performing group is related to 157-nm systems with the two stages of DOF reduction due to SSL and SSL + PDS. A typical way to interpret the curves is that 193-nm immersion systems are always better than 157-nm dry systems, stray light for stray light. Another way to look at them is the room of improvement when the illumination is polarized and SSL reduced. Table 1 lists the gain in DOF_{diff} and DOF_{avail} with TE polarized illumination at 5% exposure latitude for the common exposure-defocus (E-D) window of 32-nm lines, 90-nm and 113-nm pitches, using attenuated phase-shifting mask (AttPSM) and off-axis annular illumination (OAI). The gain in exposure latitude with DOF_{diff} kept constant at 200 nm is also shown. The gains are 23% in DOF_{diff}, 58% in DOF_{avail}, and 47% in exposure latitude.

Table 1
Poly-layer exposure latitude (ELAT) and DOF gain with polarization, 32-nm Line, 90-nm and 113-nm pitch, using attenuated phase-shift mask (AttPSM) and off-axis illumination (OAI)

AttPSM OAI	NA	Sigma	ELAT	DOFdiff	DOFavail	Improv.
Unpo	1.35	0.96:0.48	5%	137	55	
TE	1.35	0.96:0.48	5%	169	87	23/58%
Unpo	1.25	0.96:0.48	2.43%	200	118	
TE	1.25	0.96:0.48	3.57%	200	118	47%

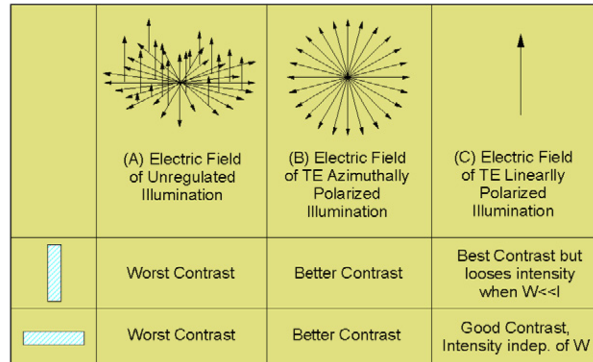

Fig. 22. Polarized illuminations to rectangular features.

TE light can be azimuthally polarized or linearly polarized as depicted in Fig. 22. The former improves the contrast of rectangular features in any orientation including horizontal and vertical ones; whereas, the latter improves the features in the same polarization orientation more than the former, but improves the features in orthogonal orientations less than the former.

5.2. *High-index materials*

Air with refractive index close to 1 has been limiting the spatial frequency coupling from the lens to the resist. Water with refractive index 1.44 at 193 nm is much better. The theoretical coupling limit sets the maximum NA of water-immersion 193-nm systems to 1.44. However, using a realistic upper limit of $\sin\theta = 0.95$ for the imaging lens, the realistic NA limit is 1.368. To break through this limit, a higher-index coupling fluid has to be used. The possibilities are depicted in Fig. 23. Staying at $\sin\theta = 0.95$, a fluid with $n = 1.56$ moves the limit to NA = 1.482. Because the refractive index of fused quartz is about 1.56 and that of CaF_2 is lower, an immersion fluid with index higher than 1.56 cannot support higher NA with a flat lens bottom. For example, at $n = 1.66$ the maximum realistic NA is still 1.482, except that due to a smaller angle in the fluid, DOF is larger. Staying with $n < 1.56$ in the lens material, the only way to increase NA beyond 1.482 is to bend the last lens surface as shown in Fig. 24. Having a non-flat bottom lens surface requires extremely low absorption in the coupling medium. Otherwise, light would be absorbed unevenly, leading to imaging difficulties. Hydro-dynamics also suffers. In order to keep the bottom lens surface flat, higher-index optical materials are needed. Though still not ready for practical applications, 193-nm immersion fluids with index ranging from 1.5 to 1.8 and lens materials with index ranging from 1.6 to 2.0 have been presented in the recent 2nd International Immersion Symposium [11–13].

5.3. *Solid mask immersion*

When the CD reaches 32 nm, it is subwavelength on the mask (0.663λ at 4X), as shown in Fig. 25. If subresolution features on the wafer are used, the features on the mask can be as small as 0.166λ. There are also subresolution 'jigs and jugs' introduced by optical proximity correction (OPC). These 3-D subwavelength features react to the illumination nonlinearly and can lead to imaging difficulties, not to mention the difficulties in making masks containing very

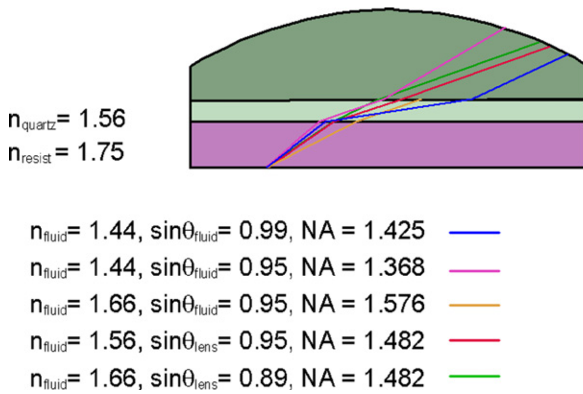

Fig. 23. Impact of fluid index.

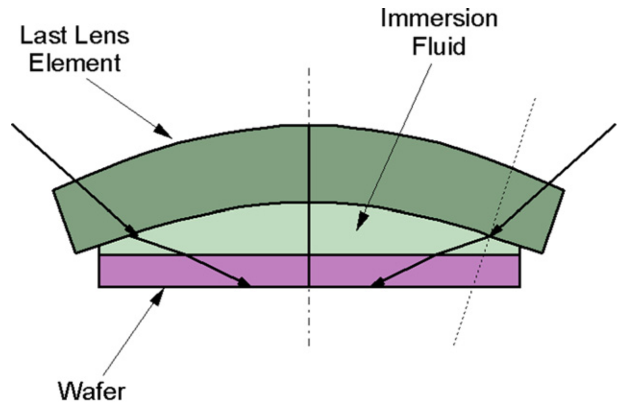

Fig. 24. Curved lens interface to sustain hyper NA.

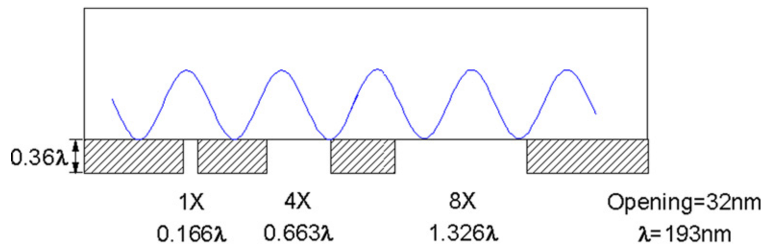

Fig. 25. 32-nm opening on 1X, 4X, 8X masks.

small features. Hence, there is motivation to increase the magnification of the mask. Furthermore, as NA becomes very large, the size of the lens, its material and fabrication costs can be unbearable. This can be alleviated by reducing the field size of the lens from the well-established standard of 26×33 mm^2. Field-size reduction and magnification increase complement each other and have attracted attention from potential beneficiaries.

The only concern on field-size reduction is the loss of productivity on the exposure tools due to a smaller field size. The time spent in stepping through smaller fields increases, thus, dropping the wafer throughput of exposure tools. A previous work [14] on productivity loss from 4X to 5X masks showed that the cost difference between 4X and 5X is about 10%. That from 4X to 8X would be significantly more. Note that in the entire semiconductor manufacturing process consisting of 30–40 masking layers, if only one layer has a tool that requires smaller field size, all other tools have to reset their field size. Price saving on tool may be on one layer but productivity loss is on all layers. Hence, productivity loss is by far the dominating factor. Mask magnification should not be increased unless prohibited by the laws of physics.

One method to delay the limitation from the laws of physics is to use a solid immersion mask as shown in Fig. 26. A high-index transparent material planarizes over the 3-D absorber structure on the mask. This way, the illuminating wavelength is reduced according to the refractive index of the planarizer. A reduction up to 70–80% is possible. Even though the wavelength is restored after light leaves the planarizer, the subwavelength diffraction zone is already taken care of. The same figure also shows improvement from experiment. The MEF is improved from 3.2 to 2.5 and DOF from 220 to 270 nm for 180 nm pitch poly-test patterns using a 500-nm thick planarizer. A thinner planarizer 200-nm thick also helps. To make this technique manufacture-worthy, the planarizing material has to withstand prolonged 193-nm radiation, can be easily and uniformly coated on the mask substrate, and can be easily removed or renewed.

5.4. Double exposure/double patterning

To further the limit, pattern pitch is a very important item to control. After the minimum pitch is reached, the limit can be extended by splitting the mask pattern into patterns of larger pitches to delineate them separately and without cross-exposure interference, onto the same areas on the wafer. The split-pitch technique is illustrated in Fig. 27. The

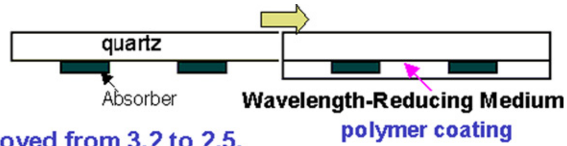

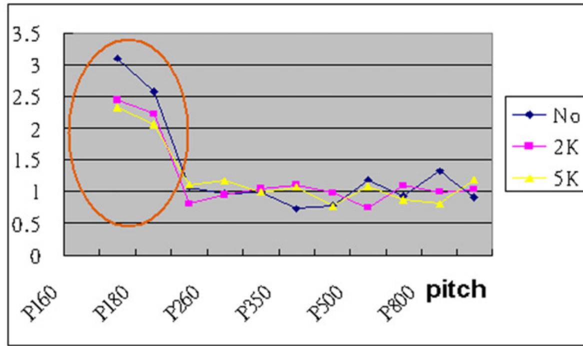

Fig. 26. Wavelength-reducing media on mask.

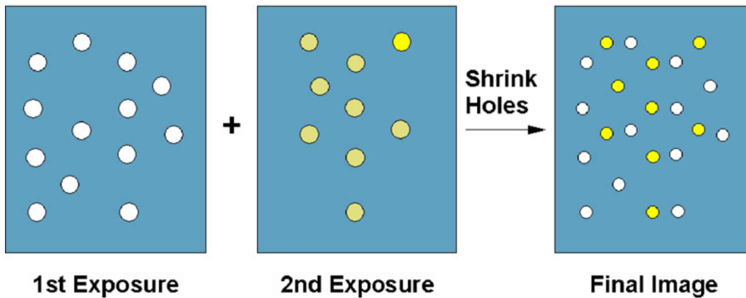

Fig. 27. Pitch splitting.

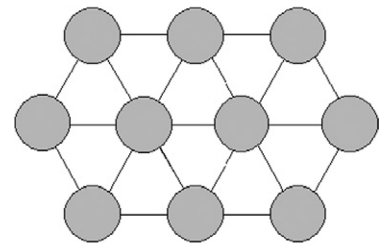

Fig. 28. Pitch splitting limit.

contact-hole pattern in the final image is split into two sets of contact holes whose size and pitch are sustainable with the imaging technology of the previous node. The size is shrunken after double exposures combine the images of the larger holes. Avoiding unacceptable interference of the two exposures is the key to the success of the split-pitch technique. Even though the interference of the two exposures is incoherent, it should still be avoided when resolution is pushed very hard. A straightforward but expensive way to do so is to develop and etch the pattern from the 1st exposure before following with the second one. A better way is to render the resist photo-insensitive, such as crosslinking, then, overcoat with another layer of resist for the 2nd exposure. The best way is to develop a resist with sufficient contrast to support double exposure.

One should be aware that the mask patterns have to be split-friendly. A simple unfriendly case is depicted in Fig. 28 where contact holes are separated by minimum distance from each other in three directions. To remove the minimum pitch, they have to be split into three masks. The bad economy of double patterning is further worsened.

The pack-unpack [15] technique uses a 2nd resist exposure to handle the cross interference issue. This double-exposure technique controls pitch by removing the less favorable pitch. In the case with contact holes, either with AltPSM or using OAI, the less favorable pitches are in the large ones and isolated holes. They suffer from small DOF. Hence, a mask with padded holes filling the gaps left by the desired holes is first exposed, followed with exposure of a 2nd mask containing unpacking features to fill the unwanted holes or reopen the desired holes. The resist image from the 1st exposure is covered with a 2nd resist layer, as shown in Fig. 29. This double-exposure technique not only

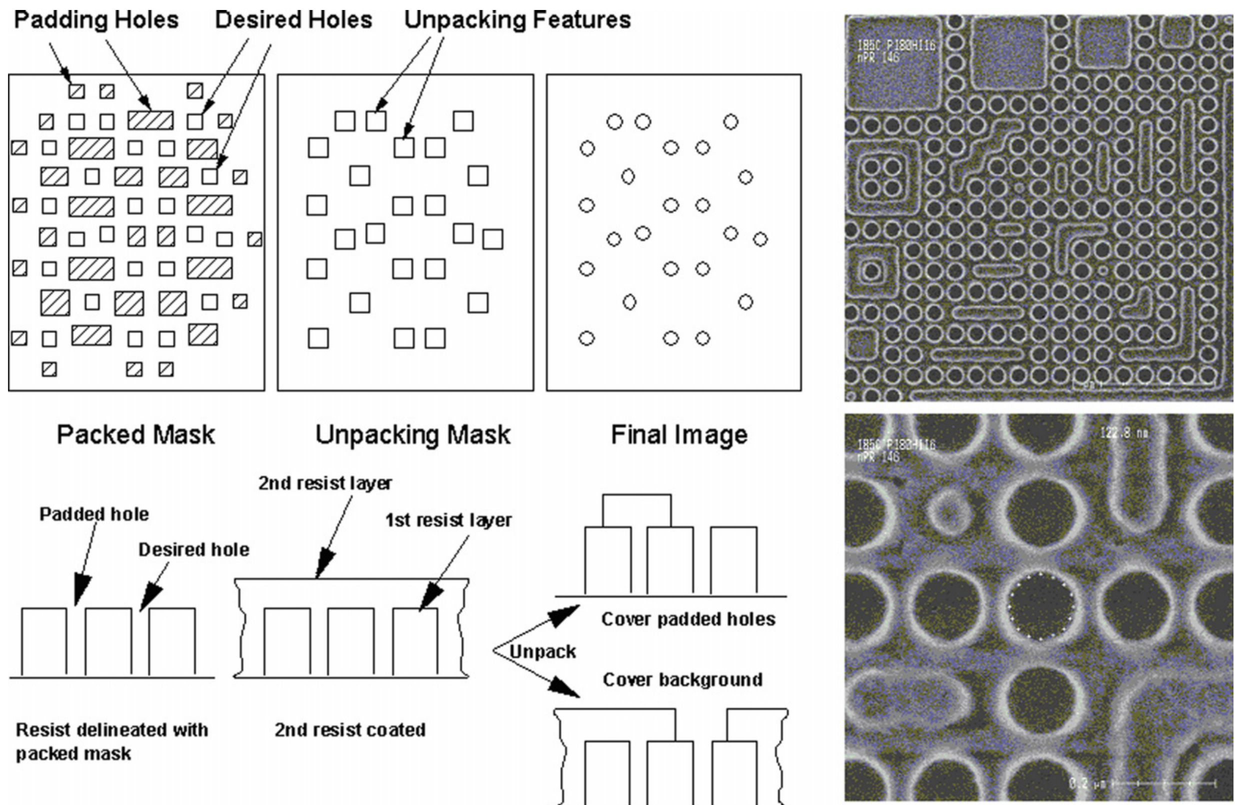

Fig. 29. Pack-unpack double exposures.

produces larger DOF. The alignment of the 2nd exposure is less critical than many other double-exposure techniques, because its function is only to remove the unwanted holes. The same figure also shows the SEM image of a working 2nd resist system. The alcohol-based resist system reported does not affect the 1st resist image. It images well, as seen in the two SEM images at two magnifications.

All double-exposure techniques have a potential to loose at least 40% of the throughput at the exposure tool, unless the tool is specifically optimized for double exposure. It is not unlikely that this will happen, unless the other lithographic systems can outperform it in imaging and cost terms.

6. Conclusions

If all the extension techniques are successful, high-index materials, polarized illumination, and solid immersion on mask supports up to $k_1 = 0.3$ at 1.55 NA and 193 nm, leading to 37-nm half pitch. Split-pitch has the potential to reduce k_1 to 0.15 from 0.3, suggesting a half pitch of 19 nm. However, the split-pitch technique requires twice as many processing steps, tools, and masks. Economy may be lost. This leaves the door open to other lithography techniques, such as extreme ultraviolet lithography, or multiple-e-beam direct write. Economy and practicality will determine its successor.

References

[1] B.J. Lin, Where is the lost resolution?, Proc. SPIE 633 (1986) 44–50.
[2] B.J. Lin, Quarter- and sub-quarter micrometer optical lithography, in: Proceedings of the Symposia on Patterning Science and Technology II, ECS 92 (6) (1991) 3.
[3] B.J. Lin, The k_3 coefficient in non-paraxial λ/NA scaling equations for resolution, depth-of-focus, and immersion lithography, J. Microlithography, Microfabrication, and Microsystems 1 (2002) 7–122.
[4] B.J. Lin, Depth of focus in multi-layered media—a long-neglected phenomenon aroused by immersion lithography, J. Microlithography, Microfabrication, and Microsystems 3 (2004) 21–27.

[5] S. Owa, H. Nagasaka, Y. Ishii, K. Shirishi, S. Hirukawa, Full-field exposure tools for immersion lithography, Proc. SPIE 5754 (2005) 655–668.
[6] B.J. Lin, Immersion lithography and its impact on semiconductor manufacturing, J. Microlithography, Microfabrication, and Microsystems 3 (2004) 377–395.
[7] F.J. Liang, L.H. Shiu, C.K. Chen, L.J. Chen, T.S. Gau, B.J. Lin, Defect reduction with special routing for immersion lithography, J. Microlithography, Microfabrication, and Microsystems, submitted for publication.
[8] J.H. Chen, L.J. Chen, T.Y. Fang, T.C. Fu, L.H. Shiu, Y.T. Huang, N. Chen, D.C. Oweyang, M.C. Wu, S.C. Wang, C.H. Lin, C.K. Chen, W.M. Chen, T.S. Gau, B.J. Lin, R. Moerman, W. Gehoel-van Ansem, E. van der Heijden, F. de Johng, D. Oorschot, H. Boom, M. Hoogendorp, C. Wagner, B. Koek, Characterization of ArF immersion process for production, Proc. SPIE 5754 (2005) 13–22.
[9] M. Switkes, M. Rothschild, Immersion lithography at 157 nm, J. Vac. Sci. Technol. B 19 (2001) 2353–2356.
[10] M. Switkes, M. Rothschild, Resolution enhancement of 157 nm lithography by liquid immersion, J. Microlithography, Microfabrication, and Microsystems 1 (2002) 225–228.
[11] S. Peng, et al., New developments in second generation 193 nm immersion fluids for lithography with 1.5 numerical aperture, in: 2nd International Symposium on Immersion Lithography, Bruges, September 2005.
[12] Y. Wang, et al., Material design for highly transparent fluids of the next generation ArF immersion lithography, in: 2nd International Symposium on Immersion Lithography, Bruges, September 2005.
[13] Y. Inui, et al., Fluoride single crystals grown by the CZ method, in: 2nd International Symposium on Immersion Lithography, Bruges, Belgium, September 2005.
[14] B.J. Lin, 4X/5X mask considerations for the future, in: ASML 157 nm Users' Forum, September 2000.
[15] D.C. Owe-Yang, S.S. Yu, H. Chen, C.Y. Chang, B.C. Ho, C.H. Lin, B.J. Lin, Double exposure for the contact layer of the 65-nm node, Proc. SPIE 5753 (2005) 171–180.